On the effects of internal heat sources upon forced convection in porous channels with asymmetric thick walls

Alexander Elliott [a], Mohsen Torabi [b], Nader Karimi [1, a], Samia Cunningham [a]

[a] School of Engineering, University of Glasgow, Glasgow G12 8QQ, United Kingdom

[b] The George W. Woodruff School of Mechanical Engineering, Georgia Institute of Technology, Atlanta, Georgia, 30332, USA

Abstract

Thermal behaviour of a porous channel with thick, solid walls featuring uneven wall thicknesses and asymmetric external thermal boundary conditions is analysed theoretically. The system is under forced convection and the fluid and solid phases in this configuration include internal heat sources with varying strengths. Two types of asymmetric boundary conditions are considered. These include constant but different prescribed temperatures on the upper and lower solid walls and a combination of constant heat flux and convective boundary conditions on the two sides of the channel. The Darcy-Brinkman model of momentum transport and the two-equation energy model are utilised to develop analytical solutions for the temperature fields and Nusselt number. A comprehensive parametric study is, subsequently, conducted. The results clearly show the pronounced effect of the internal heat sources upon the Nusselt number and temperature fields of the system. In particular, the existence of these source terms intensifies the occurrence of a bifurcation phenomenon in the temperature fields. In keeping with the recent literature, it is demonstrated that the inclusion of internal heat sources leads to deviations from the local thermal equilibrium. Nonetheless, the results imply that the extent of these deviations depends on the thermal boundary conditions and also the specific phase in which heat is generated or consumed.

Keywords: Forced convection in porous media; Internal heat sources; Local thermal non-equilibrium; bifurcation.

Nomenclature

Bi	Biot number defined in Eq. 11	T	Temperature, K
Da	Darcy number	T_1	Temperature of the lower solid material, K
h	Convection heat transfer (Case two), $\mathrm{W \cdot m^{-2} \cdot K^{-1}}$	T_2	Temperature of the upper solid material, K
h_3	Height of the channel, m	T_C	Outer temperature of the upper solid material, K
k_1	Reference thermal conductivity for lower solid material, $\mathrm{W \cdot m^{-1} \cdot K^{-1}}$	T_H	Inner temperature of the lower solid material, K
		T_f	Temperature of the fluid phase of the porous medium, K

[1] Corresponding authors:
E-mails: Nader.Karimi@glasgow.ac.uk (N.Karimi), Torabi_mech@yahoo.com (M. Torabi)

k_2	Reference thermal conductivity for upper solid material, $\mathrm{W \cdot m^{-1} \cdot K^{-1}}$
k_{ef}	Effective thermal conductivity of the fluid phase of the porous medium, $\mathrm{W \cdot m^{-1} \cdot K^{-1}}$
k_{es}	Effective thermal conductivity of the solid phase of the porous medium, $\mathrm{W \cdot m^{-1} \cdot K^{-1}}$
k_{e1}	Ratio of porous medium thermal conductivity to lower solid material thermal conductivity
k_{e2}	Ratio of porous medium thermal conductivity to upper solid material thermal conductivity
Nc	Dimensionless convection heat transfer (Case two)
Q_1	Dimensionless volumetric internal heat generation rate for the lower solid material
Q_2	Dimensionless volumetric internal heat generation rate for the upper solid material
Q_H	Dimensionless heat flux boundary condition (Case two)
w_s	Dimensionless volumetric internal heat generation rate for the solid phase of the porous medium
w_f	Dimensionless volumetric internal heat generation rate for the fluid phase of the porous medium
s_s	Volumetric internal heat generation rate for the solid phase of the porous medium
s_f	Volumetric internal heat generation rate for the fluid phase of the porous medium
$\dot{q}_1$	Volumetric internal heat generation rate for the lower solid material, $\mathrm{W \cdot m^{-3}}$
$\dot{q}_2$	Volumetric internal heat generation rate for the upper solid material, $\mathrm{W \cdot m^{-3}}$
q_H	Heat flux boundary condition (Case two), $\mathrm{W \cdot m^{-2}}$
T_s	Temperature of the solid phase of the porous medium, K
U_p	Dimensionless velocity
u_p	Velocity of the fluid in porous medium, $\mathrm{m \cdot s^{-1}}$
Y_1	Dimensionless wall thickness defined in Eq. 11
Y_2	Dimensionless wall thickness defined in Eq. 11

Greek symbols

κ	Permeability, $\mathrm{m^2}$
μ_{eff}	Dynamic viscosity of porous medium, $\mathrm{Kg \cdot s^{-1} \cdot m^{-1}}$
μ_f	Dynamic viscosity of the base fluid, $\mathrm{Kg \cdot s^{-1} \cdot m^{-1}}$
θ	Dimensionless temperature
θ_1	Dimensionless temperature of the lower solid material
θ_2	Dimensionless temperature of the upper solid material
θ_f	Dimensionless temperature of the fluid phase of the porous medium
θ_s	Dimensionless temperature of the solid phase of the porous medium
θ_H	Dimensionless temperature at outer side of the lower wall

1 Introduction

The problem of convective heat transfer in porous media has received increasing attention over the last few decades [1,2]. The growing significance of this topic can be attributed to a few reasons. These include the direct applications of transport in porous media in many conventional engineering fields such as thermal systems, chemical reactors and oil and gas reservoirs [3,4]. The subject has further found new applications in emerging fields such as biotechnology and biomedical engineering [5]. The sensitivity of these systems and the recent emphasis on improving the energy efficiencies have greatly signified the need for superior thermal models. Central to achieving this goal is the consideration of more realistic situations and, therefore, releasing the simplifying assumptions [6].

A survey of the literature reveals that a large fraction of the existing theoretical analyses in the field of forced convection in porous media includes some common simplifying assumptions [1-3]. Consideration

of local thermodynamic equilibrium, axisymmetric configurations and ignoring the internal heat sources are amongst these assumptions. Application of non-equilibrium thermodynamics has manifested itself, mostly, in the utilisation of the local thermal non-equilibrium (LTNE) or two-energy equation method [7-9]. Over the last two decades, LTNE has been applied to various flow conduits, which were fully [10-12] or partially [13-16] filled by porous materials. This has resulted in improved predictions of the temperature distribution of the individual phases in porous media. Nonetheless, the unresolved problem of thermal boundary conditions on the porous-solid and porous-fluid interfaces continues to challenge this approach [17,19,20]. Asymmetric configurations have been considered in a number of works. These often include asymmetric flow conduits partially filled by a porous insert such that the symmetry-breaking element is the location of the porous insert, see for example [21,22]. The asymmetric configurations with thick solid walls have received much less attention. The latter configuration is, generally, a lesser explored setting in the modelling of thermal systems. Recently, Ibanez et al. [23] considered the problem of heat and fluid flow in a clear micro-channel featuring thick walls. These authors [23] assumed constant thermal conductivity for the solid walls and developed analytical solutions for the momentum and energy equations. Their results clearly demonstrated the significance of thick walls in the thermal behaviour of the system [23]. The growing importance of the thermal analysis of purely conductive or conductive-convective components is also reflected by the recent research interests in this subject [24-26].

The internal heat sources in porous media under local thermal equilibrium (LTE) conditions have been included in some studies [27-29]. These works mostly concentrated on heat generation by viscous dissipation. An exception to this is the work of Chen et al. [27], which considered uniform internal heat generations under local thermal equilibrium. Examples of LTNE analyses with internal heat sources are much less frequent and mostly limited to the recent studies. In a theoretical work, Yang and Vafai [30] investigated a fully filled porous channel under LTNE condition, which also featured internal heat generations. They considered two different porous-solid thermal interface models and developed closed form analytical solutions for the temperature fields and Nusselt number [30]. Yang and Vafai demonstrated that internal heat generation could cause significant deviations from the local equilibrium condition [30]. Most recently, this work was extended to the partially filled porous channels by Karimi et al. [31] and Torabi et al. [32]. Uniform exothermic and endothermic processes were assumed to generate or consume thermal energy in the fluid and solid phases. In keeping with the earlier work of Yang and Vafai [30], these authors [31,32] showed the strong effects of internal heat sources on the thermal behaviour of the system. They also demonstrated the possibility of occurring heat flux and temperature bifurcations [31,32]. In particular, these studies confirmed the necessity of taking the non-equilibrium approach in the analysis of problems which involve internal heat sources [31,32].

In reality, there are many thermal problems in porous media which are not under local thermodynamic equilibrium, include asymmetric configurations and involve exothermic or endothermic processes. Chemical and nuclear reactors are the typical examples of this class of problems, while biological systems are another application field, in which metabolism provides the internal source of heat [33]. Biological systems are usually asymmetric and can be subject to different thermal boundary

conditions [34]. All these examples accommodate exothermic or endothermic reactions in the fluid and solid phases of the porous medium. As a result, they are likely to operate far from the local thermal equilibrium condition [35]. Further, most reactors include high pressures which necessitates using thick walls. In practice, the thickness of the wall may vary at different points resulting in an asymmetric configuration. Furthermore, reactors may be subject to various types of waves (e.g. infrared, beta and gamma waves) [36]. Absorption of these waves forms a source of thermal energy in the walls of the system. Similarly, in biological applications, the region of interest is normally surrounded by other heat generating tissues. Asymmetric porous systems with thick walls have been most recently analysed by Torabi and Zhang [37]. These authors considered magneto-hydrodynamic effects and solved the governing equations analytically to find the velocity, temperature and entropy generation rates [37]. However, their work did not include internal heat sources in the porous medium [37].

The preceding review of the literatures reveals that the thermal analysis of porous media with asymmetric configuration and internal heat sources sets a challenge that has not been previously met. In particular, the influences of internal heat sources upon the temperature and heat transfer rates are currently completely unknown. The aim of this work is to address this issue through a series of theoretical analyses.

2 Theoretical Methods

2.1 Problem Configuration and assumptions

Figure 1 shows the schematic view of the problem under investigation. The channel is fully filled by a porous material and includes thick walls with constant, but distinctive, thermal conductivities as well as constant and uniform, but dissimilar, internal heat generations. The internal heat generation within the solid walls could be, for example, the result of the absorption of gamma rays in the solid walls [38,39]. Two sets of boundary conditions are considered in this problem. In case one (Fig. 1a), it is assumed that the upper and lower surfaces are subject to constant but different temperatures. Case two (Fig. 1b) includes a constant heat flux on the lower wall and a convective boundary condition on the upper wall.

In the proceeding analyses, the classical macroscopic theory of transport in porous media [1,2] is employed and, therefore, pore scale phenomena are not investigated. The following assumptions are made throughout the current study of the porous system.

- The porous medium is homogenous and isotropic, fluid saturated and includes uniform and steady internal heat generation.
- The fluid flow is laminar, steady and incompressible, with uniform heat generation and no gravitational effects.
- The porous system is under local thermal non-equilibrium state.
- Thermally and hydrodynamically fully developed conditions hold within the porous regions.
- Due to the absence of gravity effects and assuming small emissivity, natural convection and radiation are negligible. It is, also, assumed that viscous heat generation is negligible.
- Physical properties such as porosity, specific heat, density, and thermal conductivity are invariants.

- Thermal conductivity is assumed to be constant and, therefore, thermal dispersion [40] effects are ignored here.

2.2 Governing Equations

Taking into account the assumptions made in the problem configuration, the transport of momentum in the system is expressed by the Darcy-Brinkman model, which reads,

$$-\frac{\partial p}{\partial x}+\mu_{eff}\frac{\mathrm{d}^2 u_p}{\mathrm{d}y^2}-\frac{\mu_f}{\kappa}u_p=0 \qquad h_1 \le y < h_2 \tag{1}$$

where $\mu_{eff}=\mu_f/\varepsilon$ is the effective viscosity. The transport of thermal energy within different components of the system is governed by the following equations. These represent the conduction of heat in the upper wall, transport of heat in the fluid and solid phases of the porous media and conduction of heat in the lower wall, respectively.

$$k_1\frac{\mathrm{d}}{\mathrm{d}y}\left[\frac{\mathrm{d}T_1}{\mathrm{d}y}\right]+\dot{q}_1=0 \qquad 0<y\le h_1 \tag{2}$$

$$k_2\frac{\mathrm{d}}{\mathrm{d}y}\left[\frac{\mathrm{d}T_2}{\mathrm{d}y}\right]+\dot{q}_2=0 \qquad h_2<y\le h_3 \tag{3}$$

$$k_{ef}\frac{\mathrm{d}^2 T_f}{\mathrm{d}y^2}+h_{sf}a_{sf}\left(T_s-T_f\right)+s_f=0 \qquad h_1 \le y < h_2 \tag{4}$$

$$k_{es}\frac{\mathrm{d}^2 T_s}{\mathrm{d}y^2}-h_{sf}a_{sf}\left(T_s-T_f\right)+s_s=0 \qquad h_1 \le y < h_2 \tag{5}$$

It is important to note that the assumption of fully developed flow has been incorporated in the development of Eqs. 4 and 5. The following boundary conditions are imposed on the system.

In case one:

$$y=0 \qquad T_1=T_H \tag{6a}$$

$$y=h_3 \qquad T_2=T_C \tag{6b}$$

and in case two:

$$y=0 \qquad -k_1\frac{\mathrm{d}T_1}{\mathrm{d}y}=q_H \tag{7a}$$

$$y=h_3 \qquad -k_2\frac{\mathrm{d}T_2}{\mathrm{d}y}=h\left(T_2-T_C\right) \tag{7b}$$

Both cases, further, include the following interface conditions [11],[30] ,[31]

$$y = h_1 \qquad u_p = 0 \qquad T_1 = T_s = T_f \qquad k_1 \left.\frac{\mathrm{d}T_1}{\mathrm{d}y}\right|_{y=h_1} = k_{ef} \left.\frac{\mathrm{d}T_f}{\mathrm{d}y}\right|_{y=h_1} + k_{es} \left.\frac{\mathrm{d}T_s}{\mathrm{d}y}\right|_{y=h_1} \tag{8a}$$

$$y = h_2 \qquad u_p = 0 \qquad T_2 = T_s = T_f \qquad k_2 \left.\frac{\mathrm{d}T_2}{\mathrm{d}y}\right|_{y=h_2} = k_{ef} \left.\frac{\mathrm{d}T_f}{\mathrm{d}y}\right|_{y=h_2} + k_{es} \left.\frac{\mathrm{d}T_s}{\mathrm{d}y}\right|_{y=h_2} \tag{8b}$$

In this system, the Nusselt number can be written in the form of [32]:

$$\mathrm{Nu} = -\frac{2(h_2 - h_1) \times q_w}{k_f\left(T_{f,w} - T_{f,m}\right)}, \tag{9}$$

where

$$T_{f,m} = \frac{1}{(h_2 - h_1)u_m}\left(\int_{h_1}^{h_2} u_p T_f \mathrm{d}y\right), \tag{10a}$$

$$u_m = \frac{1}{(h_2 - h_1)}\left(\int_{h_1}^{h_2} u_p \mathrm{d}y\right), \tag{10b}$$

$$q_w = k_1 \left.\frac{\partial T_1}{\partial y}\right|_{y=h_1}. \tag{10c}$$

In the limit of large convection coefficients, the temperature difference between the solid and fluid phases diminishes, and the LTE condition is approached. For conciseness reasons, the LTE formulations of the problem are not repeated here. This can be, readily, reproduced by the LTNE model formulations, following the elaborated procedure available in the literature [22].

2.3 Normalised LTNE and LTE equations

To proceed with an analytical solution of the governing equations, the following dimensionless parameters are introduced:

$$\theta_1 = \frac{T_1}{T_C} \quad \theta_s = \frac{T_s}{T_C} \quad \theta_f = \frac{T_f}{T_C} \quad \theta_2 = \frac{T_2}{T_C} \quad Y = \frac{y}{h_3} \quad Y_1 = \frac{h_1}{h_3}$$
$$Y_2 = \frac{h_2}{h_3} \quad Q_1 = \frac{\dot{q}_1 {h_3}^2}{k_1 T_C} \quad Q_2 = \frac{\dot{q}_2 {h_3}^2}{k_2 T_C} \quad Q_H = \frac{q_H h_3}{k_1 T_C} \quad w_f = \frac{s_f {h_3}^2}{k_{es} T_C} \tag{11a-t}$$
$$w_s = \frac{s_s {h_3}^2}{k_{es} T_C} \quad U_p = \frac{u_p}{u_r} \quad Da = \frac{\kappa}{{h_3}^2} \quad k = \frac{k_{es}}{k_{ef}} = \frac{(1-\varepsilon)k_s}{\varepsilon k_f}$$

$$Bi = \frac{h_{sf} a_{sf} {h_3}^2}{k_{es}} \qquad k_{e1} = \frac{k_{ef}}{k_1} \qquad k_{e2} = \frac{k_{ef}}{k_2} \qquad Nc = \frac{h h_3}{k_2}$$

where $u_r = -\frac{h_3^2}{\mu_f}\frac{\partial p}{\partial x}$. Using these parameters, the governing equations (1-5) take the following forms.

The governing momentum equation (1) becomes,

$$1 + \frac{1}{\varepsilon}\frac{\mathrm{d}^2 U_p}{\mathrm{d}Y^2} - \frac{U_p}{Da} = 0 \qquad Y_1 < Y \le Y_2 \tag{12}$$

The heat transport equations (2 - 5) reduce to,

$$\frac{\mathrm{d}}{\mathrm{d}Y}\left[\frac{\mathrm{d}\theta_1}{\mathrm{d}Y}\right] + Q_1 = 0 \qquad 0 < Y \le Y_1 \tag{13}$$

$$\frac{\mathrm{d}}{\mathrm{d}Y}\left[\frac{\mathrm{d}\theta_2}{\mathrm{d}Y}\right] + Q_2 = 0 \qquad Y_2 \le Y < 1 \tag{14}$$

$$\frac{1}{k}\frac{\mathrm{d}^2\theta_f}{\mathrm{d}Y^2} + Bi\,(\theta_s - \theta_f) + w_f = 0 \qquad Y_1 < Y \le Y_2 \tag{15}$$

$$\frac{\mathrm{d}^2\theta_s}{\mathrm{d}Y^2} - Bi\,(\theta_s - \theta_f) + w_s = 0 \qquad Y_1 < Y \le Y_2 \tag{16}$$

The normalised equations of energy and momentum now feature the following boundary conditions:

Case one:

$$Y = 0 \qquad \theta_1 = \theta_H \tag{17a}$$

$$Y = 1 \qquad \theta_2 = 1 \tag{17b}$$

Case two:

$$Y = 0 \qquad -\frac{\mathrm{d}\theta_1}{\mathrm{d}Y} = Q_H \tag{18a}$$

$$Y = 1 \qquad -\frac{\mathrm{d}\theta_2}{\mathrm{d}Y} = Nc\left(\theta_2 - 1\right). \tag{18b}$$

The dimensionless interface conditions are written as

$$Y = Y_1 \quad U_p = 0 \quad \theta_1 = \theta_s = \theta_f \quad \left.\frac{\mathrm{d}\theta_1}{\mathrm{d}Y}\right|_{Y=Y_1} = k_{e1}\left.\frac{\mathrm{d}\theta_f}{\mathrm{d}Y}\right|_{Y=Y_1} + k\,k_{e1}\left.\frac{\mathrm{d}\theta_s}{\mathrm{d}Y}\right|_{Y=Y_1} \tag{19a}$$

$$Y = Y_2 \quad U_p = 0 \quad \theta_2 = \theta_s = \theta_f \quad \left.\frac{\mathrm{d}\theta_2}{\mathrm{d}Y}\right|_{Y=Y_2} = k_{e2}\left.\frac{\mathrm{d}\theta_f}{\mathrm{d}Y}\right|_{Y=Y_2} + k\,k_{e2}\left.\frac{\mathrm{d}\theta_s}{\mathrm{d}Y}\right|_{Y=Y_2} \tag{19b}$$

The energy equations for the solid walls (Eqs. (13) and (14)) are linear and uncoupled. Hence, they can be solved with relative simplicity. For the porous region, the energy equations are coupled and should be decoupled before they can be solved analytically. Differentiating and combining Eqs. (15) and (16) leads to the following fourth-order differential equations,

$$\theta_s''''(Y) - \mathrm{Bi}(k+1)\theta_s''(Y) - \mathrm{Bi}k\left(w_f + w_s\right) = 0 \tag{20}$$

$$\theta_f''''(Y) - \mathrm{Bi}(k+1)\theta_f''(Y) - \mathrm{Bi}k\left(w_f + w_s\right) = 0 \tag{21}$$

Further, using the dimensionless parameters listed in relations (11a-t) the dimensionless Nusselt number is given by the following relations,

$$\mathrm{Nu} = -\frac{2\varepsilon(Y_2 - Y_1) \times \left.\frac{\partial\theta_1}{\partial y}\right|_{Y=Y_1}}{k_{e1}\left(\theta_f(Y_1) - \theta_{f,m}\right)}, \tag{22}$$

where,

$$\theta_{f,m} = \frac{1}{(Y_2 - Y_1)U_m}\left(\int_{Y_1}^{Y_2} U_p\theta_f \mathrm{dY}\right) \tag{23a}$$

$$U_m = \frac{1}{(Y_2 - Y_1)}\left(\int_{Y_1}^{Y_2} U_p \mathrm{dY}\right) \tag{23b}$$

Application of the LTE model on the same system leads to the development of the following energy equations:

$$\frac{\mathrm{d}}{\mathrm{d}Y}\left[\frac{\mathrm{d}\theta_1}{\mathrm{d}Y}\right] + Q_1 = 0 \quad 0 < Y \le Y_1 \tag{24a}$$

$$\left(\frac{1}{k}+1\right)\frac{\mathrm{d}^2\theta_f}{\mathrm{d}Y^2} + w_f + w_s = 0 \quad Y_1 < Y \le Y_2 \tag{24b}$$

$$\frac{\mathrm{d}}{\mathrm{d}Y}\left[\frac{\mathrm{d}\theta_2}{\mathrm{d}Y}\right] + Q_2 = 0 \quad Y_2 \le Y < 1, \tag{24c}$$

where in this system $\theta_f = \theta_s$ due to the local equilibrium assumption. The upper and lower boundary conditions of the system considering LTE model is similar to the stated conditions in LTNE model. However, the coupling conditions between the walls and porous medium are changed to the following relations.

$$Y = Y_1 \qquad \theta_1 = \theta_f \qquad \left.\frac{\mathrm{d}\theta_1}{\mathrm{d}Y}\right|_{Y=Y_1} = \left(k_{e1} + k\ k_{e1}\right)\left.\frac{\mathrm{d}\theta_f}{\mathrm{d}Y}\right|_{Y=Y_1} \tag{25a}$$

$$Y = Y_2 \qquad \theta_1 = \theta_f \qquad \left.\frac{\mathrm{d}\theta_2}{\mathrm{d}Y}\right|_{Y=Y_2} = \left(k_{e2} + k\ k_{e2}\right)\left.\frac{\mathrm{d}\theta_f}{\mathrm{d}Y}\right|_{Y=Y_2} \tag{25b}$$

The solution of the LTE model is considerably simpler than the LTNE model and provides a tool to verify the correctness of the developed solutions for the LTNE model. This is discussed in the following section.

2.4 Temperature and velocity profiles

Solving the dimensionless momentum Eq. (12), together with the boundary conditions detailed in Eq. (19), yields the following fluid velocity profile:

$$U_p(Y) = -\frac{4\mathrm{Da}\left(\sinh\left(\frac{Z}{2}(Y-Y_1)\right)\sinh\left(\frac{Z}{2}(Y-\mathrm{Y2})\right)\left(\sinh\frac{Z}{2}(Y_1+\mathrm{Y2})+\cosh\left(\frac{Z}{2}(Y_1+\mathrm{Y2})\right)\right)\right)}{\sinh(\mathrm{Z}Y_1)+\cosh(\mathrm{Z}Y_1)+\sinh(\mathrm{Z}Y_2)+\cosh(\mathrm{Z}Y_2)} \tag{26}$$

Solving Eqs. (13) and (14), as well as Eqs. (20) and (21), results in the following general solutions for the temperature profiles of the porous region and the solid walls,

$$\theta_s(Y) = E_s Y^2 + F_s\cosh(Y\Gamma) + K_{1s}Y + K_{2s} \tag{27a}$$

$$\theta_f(Y) = E_f Y^2 + F_f\cosh(Y\Gamma) + +K_{1f}Y + K_{2f} \tag{27b}$$

$$\theta_1(Y) = A_1 Y^2 + B_1 Y + C_1 \tag{27c}$$

$$\theta_2(Y) = A_2 Y^2 + B_2 Y + C_2 \tag{27d}$$

Application of the boundary conditions (17)-(19) leads to the specification of the constant parameters in Eqs. (27a-d) and reveals the particular solution. Finding these parameters requires a significant amount of algebraic manipulation. Hence, Wolfram Mathematica was used to complete this part of the analytical solution. The resultant constant parameters are quite long and complicated, and, therefore, are not shown here. The Nusselt number can be readily attained through substitution of the temperature and velocity solutions into Eqs. (22) and (23). Once again, for reasons of brevity, the full form has been omitted.

3 Results and Discussion

This section is divided into two subsections. First, a validation of the temperature solutions is provided and a comprehensive discussion about the temperature distribution within the system is put forward. This is followed by the evaluation of Nusselt number versus various pertinent parameters, in the second subsection. It should be noted that, since the velocity field and its relevant discussion is straightforward, this has not been elaborated here. Further, in the proceeding discussions, parts a and b of each figure always correspond to cases one and two shown in Fig 1a and 1b, respectively.

3.1 Temperature Distribution

It is known that increasing the Biot number to a large enough value should result in the conversion of LTE and LTNE solutions. This is due to the fact that, at large Biot numbers, the internal heat exchanges within the porous media are strong. Hence, thermal equilibrium condition is favoured. The LTNE model of the problem has been provided in section 2.3 and the resultant equations for temperature, Eqs. (27), have been implemented with a high value of Biot number, i.e. Bi = 100, in Fig. 2a. This can be repeated for case two (Fig. 1b) and the results are illustrated in Fig. 2b. As these two figures demonstrate, in the limit of large Biot numbers, the LTNE solution agrees with the LTE model very well, assuring the correctness of the current analytical work.

Fig. 3 shows the temperature profile for the entire channel employing a range of values for the Biot number. In both cases, it is clear that an increase in the Biot number reduces the temperature difference between the solid and fluid phases inside the porous region. Fig. 3a also demonstrates the influence of Biot number on the solid walls temperatures in the first case. Interestingly, in the second case, when the temperatures of the upper and lower walls are not fixed, the temperatures of the walls are practically independent of Biot number.

The influence of the thermal conductivity ratio, k, is shown in Fig. 4. In both Figs. 4a and 4b, it can be seen that increasing the value of this variable increases the non-equilibrium effect. That is, the difference between the solid and fluid phases in the porous region is increased. When the thermal conductivity ratio is equal to 1, and hence the solid and fluid effective conductivities are equal to each other, this difference is entirely eliminated. Under this condition, the porous region can be effectively considered to be under LTE. Most importantly, by increasing the thermal conductivity ratio from less than unity to more than one, a bifurcation phenomenon occurs in the temperature fields of the porous medium. In Figs. 4a and b and for k=0.5, at any value of Y the solid phase of the porous medium is hotter than the fluid phase. However, for the values of k greater than one, this trend is reversed and fluid phase becomes hotter. It follows that the direction of the internal heat exchange between the two phases can be reversed as a result of variations in the relative thermal conductivities. This bifurcation phenomenon has been most recently reported in simpler configurations [32]. Nonetheless, the current results are the first observation of this phenomenon in thick walls, heat generating porous channels. Further, in both cases (Figs. 4a and b) the thermal conductivity ratio can be also seen to affect the solid wall temperatures. Fig. 4b demonstrates that, when non-fixed temperature boundary conditions are in place, this ratio can significantly affect the boundary temperature of the two walls.

Figures 5 and 6 show, respectively, the effects of internal heat generation and consumption in the fluid and solid phases of the porous region. As shown in Fig. 5 and 6 the exothermicity and

endothermicity characteristics of the porous region can have strong effects on the temperature profiles of this system. Occurrence of temperature bifurcation phenomena in Figs. 5 and 6 is evident. In these figures, internal heat sources within the porous region are kept limited to one phase. In Fig. 5, in which internal heat sources are limited to fluid phase, endothermic fluid is always colder than the solid phase of the porous medium. However, the temperature of the exothermic fluid exceeds that of the solid in the two investigated cases. Analogous statements can be developed for Figs. 6a and b. Furthermore, Fig. 5 includes three major features induced by the internal heat sources. First, it is clear from Fig. 5a and b that the temperature difference between the solid and fluid phases in the porous medium is heavily dependent upon the strength of the internal heat sources. This is such that, when these source terms are set to zero, there is little temperature difference between the two phases and, therefore, the LTE condition holds. Second, a comparison between Figs. 5a and 5b indicates that the temperature difference between the solid and fluid phases is, generally, smaller in Fig. 5b. This implies the significance of thermal boundary conditions in the deviation of the system from LTE. Third, Fig. 5b shows that in case two, internal heat sources in the porous region can majorly influence the boundary temperatures of the solid walls. This is similar to the effect of thermal conductivity ratio as examined in Fig. 4. A similar discussion can be made for Fig. 6 and, hence, is not repeated. However, it is worth noting that the extent of temperature differences in Fig. 6 is smaller than the corresponding ones in Fig. 5. This indicates the superior role of heat generation within the fluid phase in the thermal behaviour of the system.

Figures 7-9 demonstrate the variation of the temperature profile as a result of variations in the boundary conditions. These include the hot boundary temperature in case one (Fig. 7), heat convection coefficient (Fig. 8) and imposed heat flux (Fig. 9) boundary conditions in case two. Varying the temperature of the lower wall in case one, see Fig. 7, impacts the temperature profile of the entire system. However, the magnitude of the temperature difference in the porous region is not noticeably affected by the variation in θ_H. Similar behaviour can be also noted in Fig. 8 and Fig. 9, in which neither varying the convection nor the heat flux boundary conditions affect the inter-phase temperature differences. A comparison between Figs. 7, 8 and 9 reveals that, in general, the deviation from local thermal equilibrium is more significant in case one. Further, for the range of parameters used in these figures, the fluid phase always remains the hotter phase.

3.2 Nusselt Number

Fig. 10 shows the variation of Nusselt number versus Darcy number, with both Fig. 10a and Fig. 10b showing little variation of Nusselt number as Darcy number is increased. This implies that, in the current problem, the effects of permeability on the heat transfer characteristics are almost negligible. However, the porosity of the medium appears to have a significant influence on the Nusselt number. This is such that increasing the porosity from 0.5 to 0.9 in Fig. 10 almost doubles the value of Nusselt number. For both cases 1 and 2 (shown in Fig. 10a and b), increasing the porosity of the medium results in increasing the Nusselt number. The effects of thermal conductivity ratio upon the Nusselt number are shown in Fig. 11. It is clear from this figure that the thermal boundary conditions in cases 1 and 2 can have major influences upon the qualitative behaviour of Nusselt number against the thermal conductivity ratio. Figure 11a shows that, for a given porosity, the maximum value of Nusselt number is achieved at k= 1.

Deviations from this value leads to a drop in Nusselt number. However, case two presents a distinctive behaviour in which increasing k leads to a monotonic reduction of the Nusselt number. Further, in both Fig. 11a and b, by increasing the porosity, the extent of Nusselt number variation with k increases. It follows that, at very low porosities (not shown here), the Nusselt number becomes almost indifferent to the thermal conductivity ratio. Figure 12 shows that the thickness of the lower solid wall can impart considerable effects upon the numerical value of the Nusselt number. In case one (Fig. 12a), thickening this wall, generally, increases the Nusselt number. However, the reverse trend is observed in case two (Fig. 12b). Similar to that observed in Fig. 11, the extent of variation increases as the porosity of the medium increases. It is interesting to note that, at high values of porosity, tripling the wall thickness can result in almost 20% enhancement of the Nusselt number, see Fig. 12a. A similar behaviour is observed in Fig. 13, which shows the variations of Nusselt number against the upper wall thickness for the two investigated cases. The general trend in this figure is the opposite of that in Fig. 12, and, in case one the Nusselt number decreases with increasing Y_2. However, increases in the thickness of the top wall (Y_2), in Fig. 13b, results in the growth of Nusselt number. The findings of Figs. 12 and 13 are of immediate practical significance, and reflect the importance of the wall thickness in determining the heat transfer characteristics of the system.

Figures 14 and 15 illustrate the impacts of internal heat sources in the porous medium (ω_f, ω_s) upon the heat convection coefficient. In Figs. 14a and b, the fluid internal heat source is varied widely from endothermic to exothermic state, while the internal heat generation in the solid is set to zero. It is clear from these figures that internal heat source in the fluid phase can have a very pronounced effect on the Nusselt number. Generally, in both cases one and two (Figs. 14a and b), Nusselt number is directly correlated with ω_f. This correlation exists over the entire investigated range of ω_f. Nonetheless, it is stronger in exothermic fluids. This is particularly true for case one (Fig. 14a), which presents a sharp gradient of changes in Nu number versus ω_f in the exothermic region ($\omega_f > 0$). In contrast with that discussed for the fluid exothermicity/endothermicity, Fig. 15 shows that any increase in the value of ω_s results in the reduction of the Nusselt number. This trend is stronger for the endothermic solid phase under case two (see the left part of Fig. 15b). In keeping with the earlier findings of this work, Fig. 15 shows that the value of Nusselt number increases as the porosity becomes larger. Figures 14 and 15 clearly demonstrated that relatively small changes in the internal heat sources can lead to an increase/decrease of the Nusselt number by an order of magnitude. Amongst the parameters investigated in this work, this sensitivity is only comparable to the effects of the thermal conductivity ratio.

4 Conclusions

A two-dimensional channel with non-symmetric, thick solid walls, filled with a porous medium was considered. The porous part of the channel included a steady, laminar, fully-developed flow of a constant fluid density. It was further assumed that the system is under LTNE and that internal heat generation can occur in both solid and fluid phases. Two sets of boundary conditions were considered. The first assumed that the outer walls had a fixed temperature, with the lower wall having the higher temperature of the two. The second configuration included a constant heat flux on the lower wall and a convection condition

at the upper boundary. Analytical solutions for the velocity and temperature profiles, and Nusselt number within the channel were developed. It was shown that internal heat generation or consumption (exothermicity or endothermicity) can significantly affect the state of local equilibrium within the porous region. The main findings of this work can be summarised as follows.

- It was demonstrated that the Nusselt number can be significantly dependent upon the internal heat generations in the fluid and solid phases (ω_f and ω_s).
- Nusselt number is also a strong function of the wall thicknesses and therefore the geometry of the channel is an important parameter affecting the thermal behaviour of the system.
- For a fixed geometry, the thermal boundary conditions on the external surfaces of the system can majorly alter the heat transfer characteristics of the system.
- In keeping with other recent works [31, 32], this study showed the general necessity of using LTNE for the analysis of the problems with internal heat generation. However, the results imply that the asymmetry of the problem may affect the extent of deviation from LTE, and the boundary conditions can modify the local temperature differences in the porous region.
- It appears that the internal heat source in the fluid phase has a stronger influence upon the local temperature differences in the porous region. However, solid and fluid internal heat sources have similar extents of influence on the Nusselt number.

These findings are deemed to have direct applications in engineering analysis of the porous systems with thick walls. Further, the results of this investigation can be, also, used for the validation of future numerical and theoretical analyses.

References

[1] Nield, D. A., Adrian B., Convection in porous media, Springer, New York, 2013.

[2] Vadasz, P. (Ed.), Emerging Topics in Heat and Mass Transfer in Porous Media, Springer, Berlin, 2008.

[3] Ingham, D.B., Pop I. (Eds.), Transport Phenomena in Porous Media III, Elsevier, Oxford, 2005.

[4] Vafai K., Handbook of porous media, Marcel Dekker, Ohio, 2000.

[5] Vafai, K., Porous Media: Applications in Biological Systems and Biotechnology, CRC Press, Boca Raton, FL, 2011.

[6] Luo, L., Heat and Mass Transfer Intensification and Shape Optimization - A Multi-scale Approach. Springer, New York, 2013.

[7] Yang, C., Ando K., Nakayama A., A Local thermal non-equilibrium analysis of fully developed forced convective flow in a tube filled with a porous medium, Transport in Porous Media 2011; 89, 237–249.

[8] Lee, D.Y., Vafai K., Analytical characterization and conceptual assessment of solid and fluid temperature differential in porous media, International Journal of Heat and Mass Transfer 1999, 42, 423-435.

[9] Khashan, S.A., Al-Amiri A.M., Al-Nimr M.A., Assessment of the local thermal non-equilibrium condition in developing forced convection flows through fluid-saturated porous tubes, Applied Thermal Engineering 2005; 25, 1429–1445.

[10] Ouyang, X.L., Vafai K., Jiang P.X., Analysis of thermally developing flow in porous media under local thermal non-equilibrium conditions, International Journal of Heat and Mass Transfer 2013; 67, 768–775.

[11] Alazmi B., Vafai K., Analysis of variants within the porous media transport models, Journal of Heat Transfer 2000; 122(2), 303-326.

[12] Kim, S.J., Jang S.P., Effects of the Darcy number, the Prandtl number, and the Reynolds number on local thermal non-equilibrium, International Journal of Heat and Mass Transfer 2002; 45, 3885–3896.

[13] Mahmoudi, Y., Karimi N., Numerical investigation of heat transfer enhancement in a pipe partially filled with a porous material under local thermal non-equilibrium condition, International Journal of Heat Mass Transfer 2014; 68, 161–173.

[14] Mahmoudi, Y., Karimi N., Mazaher, K., Analytical investigation of heat transfer enhancement in a channel partially filled with a porous material under local thermal non-equilibrium condition: Effects of different thermal boundary conditions at the porous-fluid interface, International Journal of Heat and Mass Transfer 2014; 70, 875–891.

[15] Karimi, N., Mahmoudi Y., Temperature fields in a channel partially-filled with a porous material under local thermal non-equilibrium condition-an exact solution, Proceedings of the Institution of Mechanical Engineering, Part C, Journal of Mechanical Engineering Science 2014; 228(15), 2778-2789.

[16] Nimvari, M.E., Maerefat M., El-Hossaini M.K., Numerical simulation of turbulent flow and heat Transfer in a channel partially filled with a porous media, International Journal of Thermal Sciences 2012, 60:131-141.

[17] Seddiq, M., Maerefat M., Mirzaei M., Modeling of heat transfer at the fluid–solid interface by lattice Boltzmann method. International Journal of Thermal Sciences 2014, 75 :28-35.

[18] Vafai, K.R., Thiyagaraja R., Analysis of flow and heat transfer at the interface region of a porous medium, International Journal of Heat and Mass Transfer 1987; 30, 1391-1405.

[19] Alazmi, B., Vafai K., Analysis of fluid flow and heat transfer interfacial conditions between a porous medium and a fluid layer, International Journal of Heat and Mass Transfer 2001, 44, 1735-1749.

[20] Imani, G. R., Maerefat M., Hooman K., Estimation of heat flux bifurcation at the heated boundary of a porous medium using a pore-scale numerical simulation, International Journal of Thermal Sciences 2012, 54 : 109-118.

[21] Kuznetsov, A.V., Nield D.A., Forced convection in a channel partly occupied by a bidisperse porous medium: asymmetric case. International Journal of Heat and Mass Transfer 2010, 53.23: 5167-5175.

[22] Torabi, M., Zhang K., Yang G., Wang J., Wu P., Heat transfer and entropy generation analyses in a channel partially filled with porous media using local thermal non-equilibrium model, Energy 2015, 82 : 922-938.

[23] Ibáñez, G., López A., Pantoja J., Moreira J., Reyes J.A., Optimum slip flow based on the minimization of entropy generation in parallel plate microchannels, Energy 2013 50: 143-149.

[24] Torabi, M., Aziz A., Zhang K., A comparative study of longitudinal fins of rectangular, trapezoidal and concave parabolic profiles with multiple nonlinearities, Energy 2013, 51: 243-256.

[25] Torabi, M., Zhang K., Yang G., Wang J., Wu P., Temperature distribution, local and total entropy generation analyses in asymmetric cooling composite geometries with multiple nonlinearities: Effect of imperfect thermal contact, Energy 2014, 78: 218-234.

[26] Torabi, M., Zhang K., Classical entropy generation analysis in cooled homogenous and functionally graded material slabs with variation of internal heat generation with temperature, and convective–radiative boundary conditions, Energy 2014, 65: 387-397.

[27] Chen, G. M., Tso C.P., Hung Y.M., Field synergy principle analysis on fully developed forced convection in porous medium with uniform heat generation, International Communications in Heat and Mass Transfer 2011, 38 9 : 1247-1252.

[28] K. Hooman, Gurgenci H., Effects of viscous dissipation and boundary conditions on forced convection in a channel occupied by a saturated porous medium, Transport in Porous Media 2007, 68: 301–319.

[29] Y.M. Hung, Tso C.P., Temperature variations of forced convection in porous media for heating and cooling processes: internal heating effect of viscous dissipation, Transport in Porous Media 2008, 75: 319–332.

[30] Yang, K., Vafai K., Analysis of temperature gradient bifurcation in porous media – an exact solution, International Journal of Heat Mass Transfer 2010; 53, 4316–4325.

[31] Karimi, N., Agbo D., Talat Khan A., Younger P.L., On the effects of exothermicity and endothermicity upon the temperature fields in a partially-filled porous channel, International Journal of Thermal Sciences 2015;96:128–48.

[32] Torabi, M., Karimi N., Zhang K., Heat transfer and second law analyses of forced convection in a channel partially filled by porous media and featuring internal heat sources, Energy 2015, 93.1: 106-127

[33] Mahjoob, S., Vafai K., Analysis of bioheat transport through a dual layer biological media. Journal of Heat Transfer 2010, 132.3: 031101.

[34] Mahjoob, Shadi, and Kambiz Vafai. Analytical characterization of heat transport through biological media incorporating hyperthermia treatment, International Journal of Heat and Mass Transfer 2009, 52.5: 1608-1618.

[35] Oliveira, A.A.M., Kaviany M., Nonequilibrium in the transport of heat and reactants in combustion in porous media, Progress in Energy and Combustion Science 2001, 27.5: 523-545.

[36] Iitsuka, Y., Yamauchi H., Sato S., Takashima K., Mizuno A., Prieto G., Ammonia production from solid urea using nonthermal plasma. Industry Applications, IEEE Transactions on 2012, 48.3: 872-877.

[37] Torabi, M., Zhang K., Temperature distribution, local and total entropy generation analyses in MHD porous channels with thick walls, Energy 2015, 87: 540-554.

[38] Claiborne, H.C., Solomito M., Ritts J.J., Heat generation by neutrons in some moderating and shielding materials. Nucl Eng Des 1971;15:232–6.

[39] Ma, B.M. Heat generation and temperature distributions in cylindrical reactor pressure vessels. Nucl Eng Des 1969;11:1–15.

[40] Amiri, A., Vafai K., Analysis of dispersion effects and non thermal equilibrium, non Darcian, variable porosity, in compressible flow through porous media, International Journal of Heat and Mass Transfer 1994, 37: 939-954.

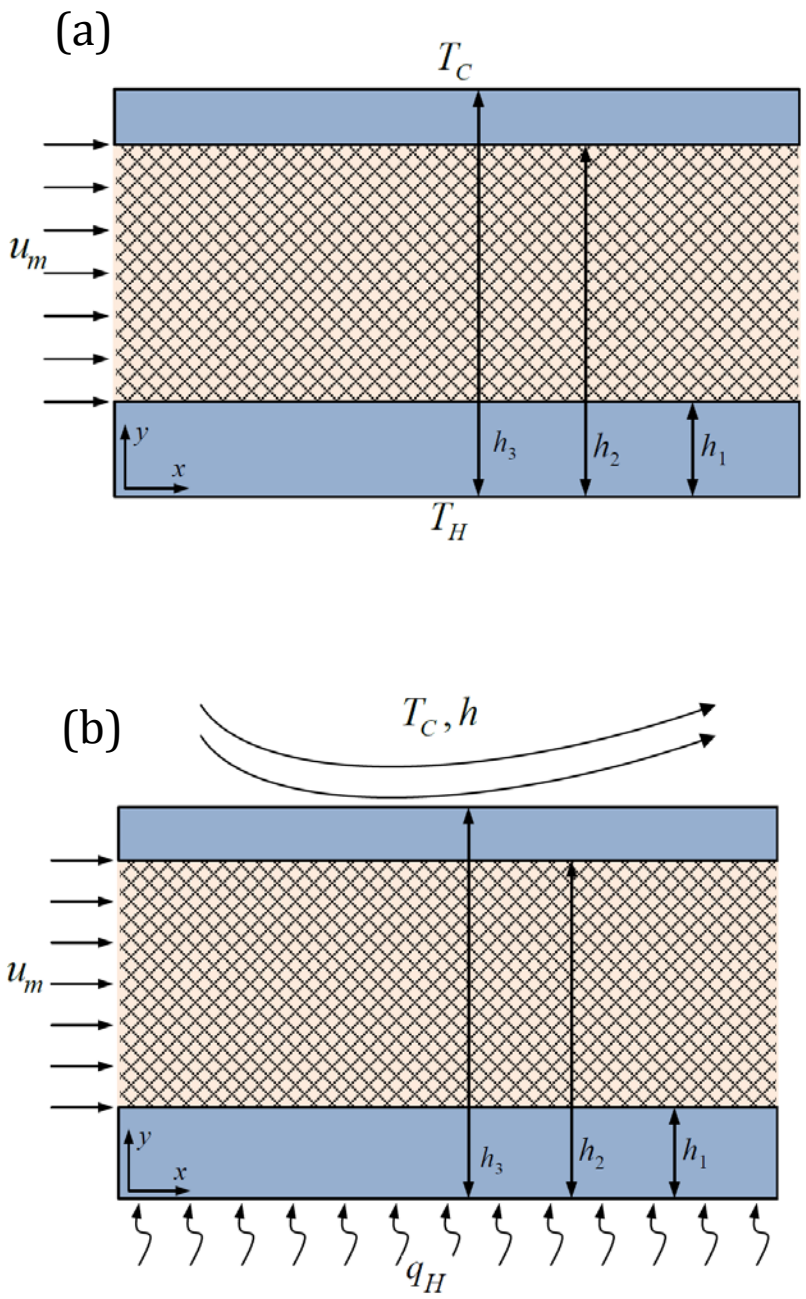

Fig. 1. Configuration of the channel filled with a porous material for (a) Case one and (b) Case two.

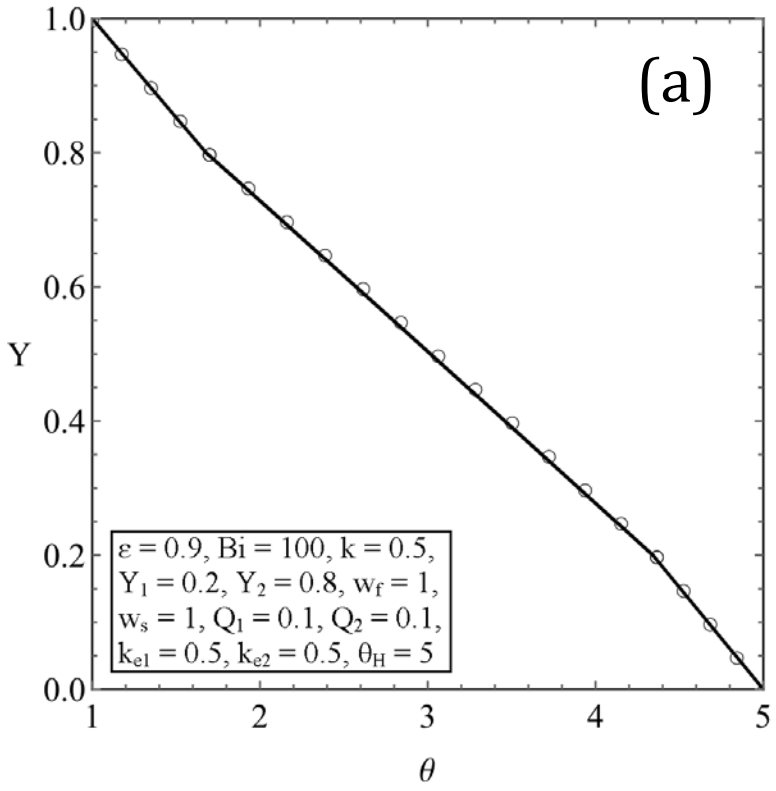

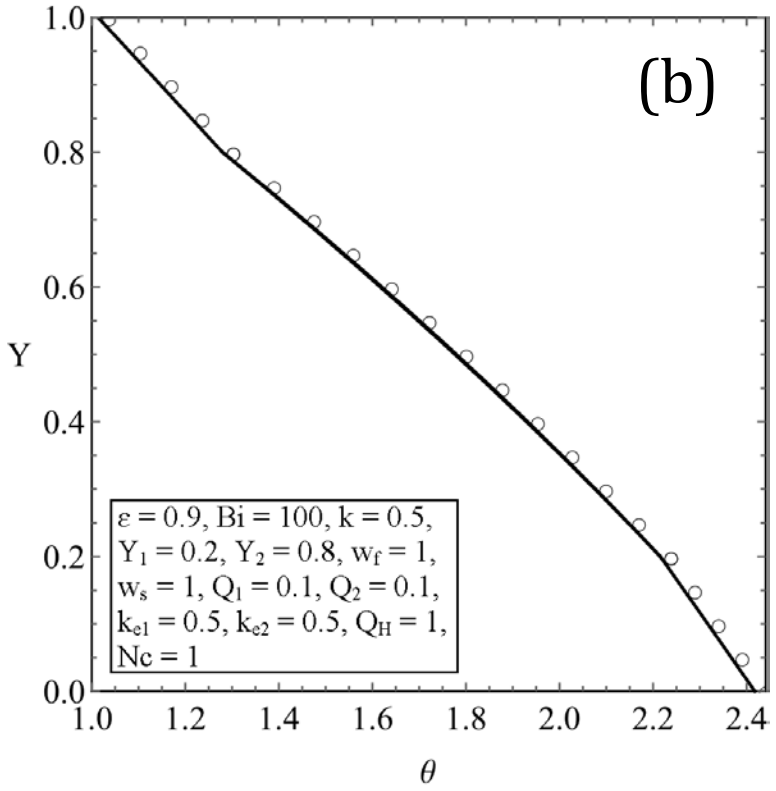

Fig. 2. Comparison between the LTNE (solid line) and LTE (circles) solutions of temperature for (a) Case one and (b) Case two.

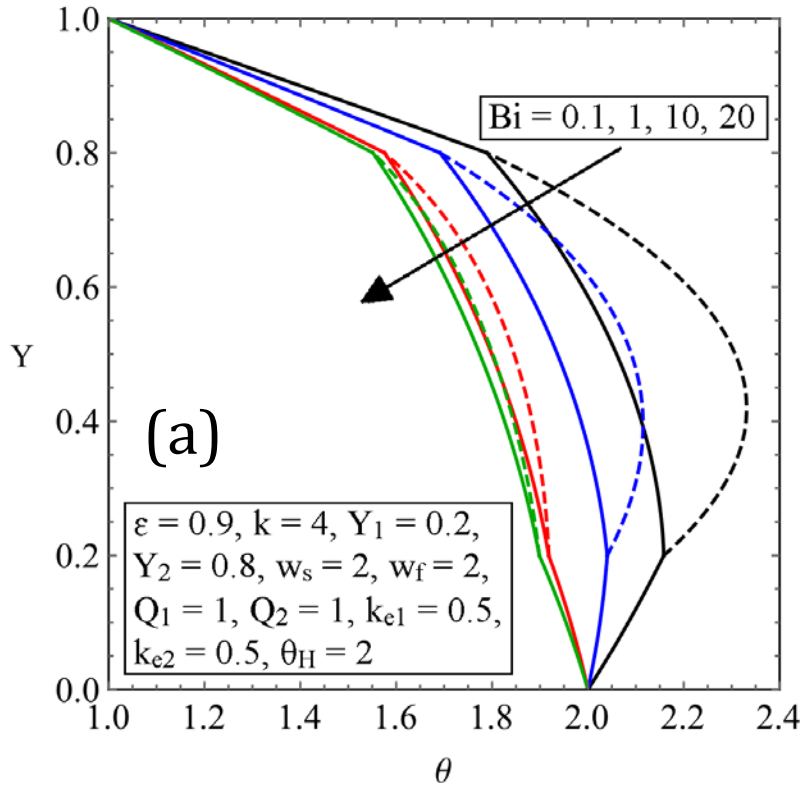

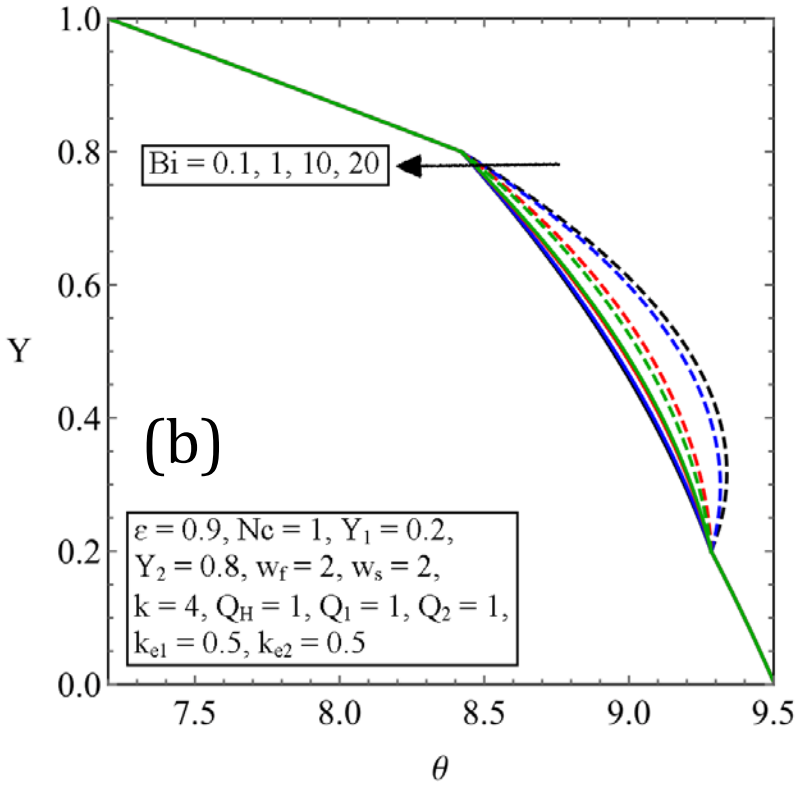

Fig. 3. Temperature distribution with various values of Biot number: (a) Case one, (b) Case two.

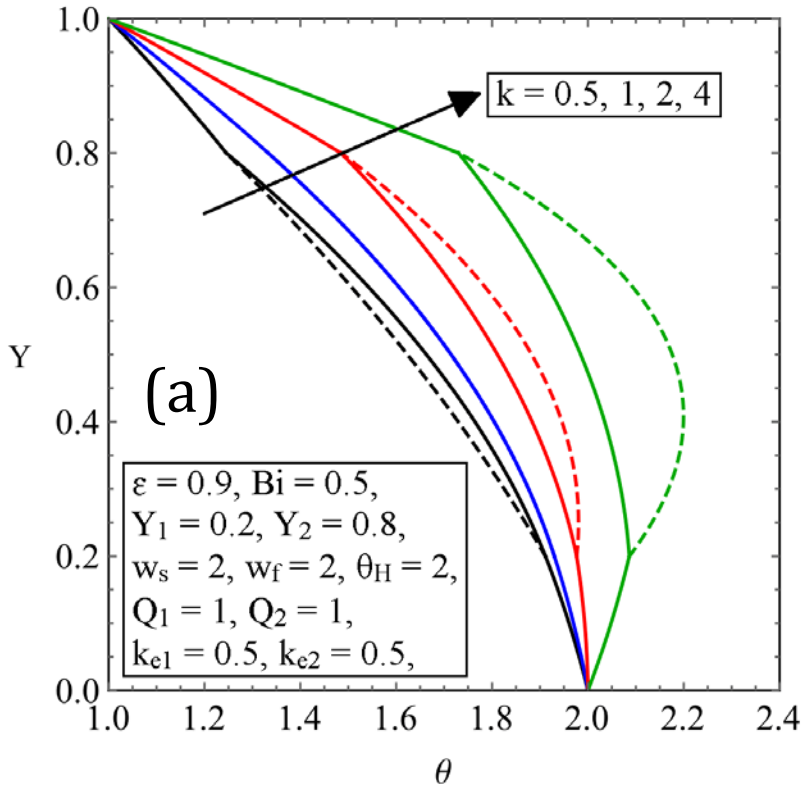

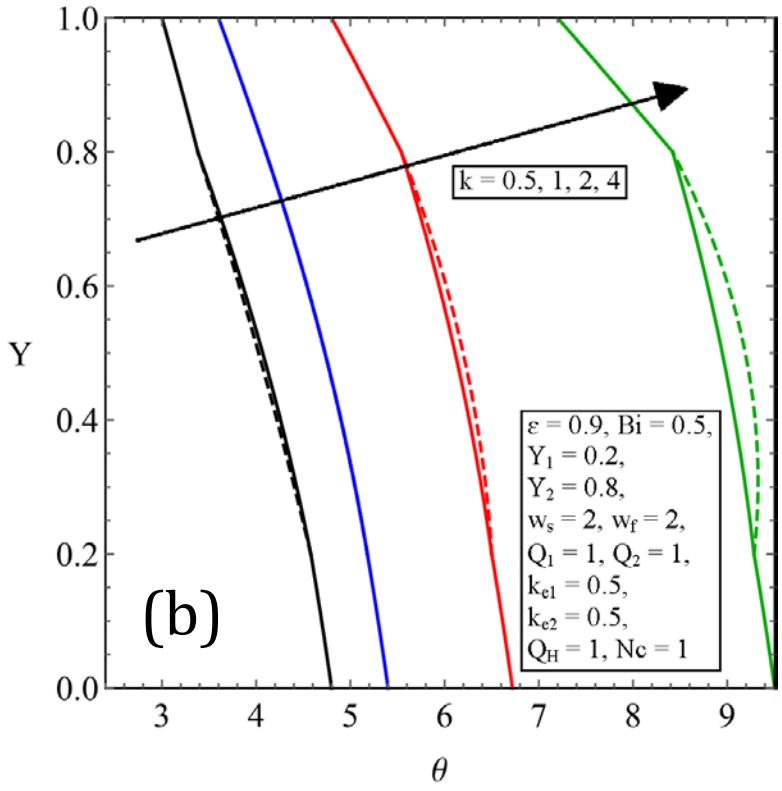

Fig. 4. Temperature distribution with various values of thermal conductivity ratio: (a) Case one, (b) Case two.

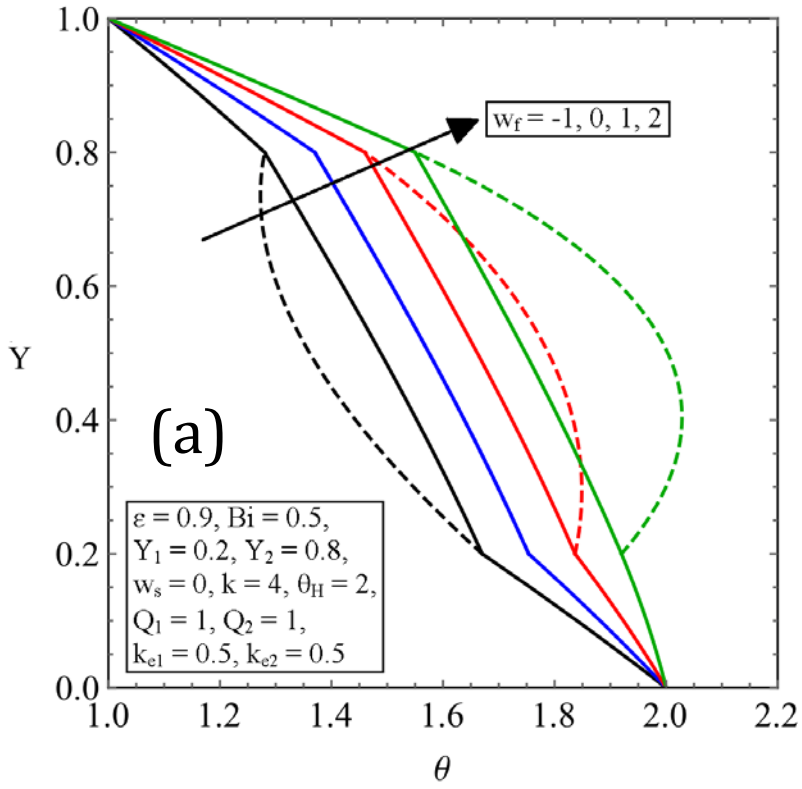

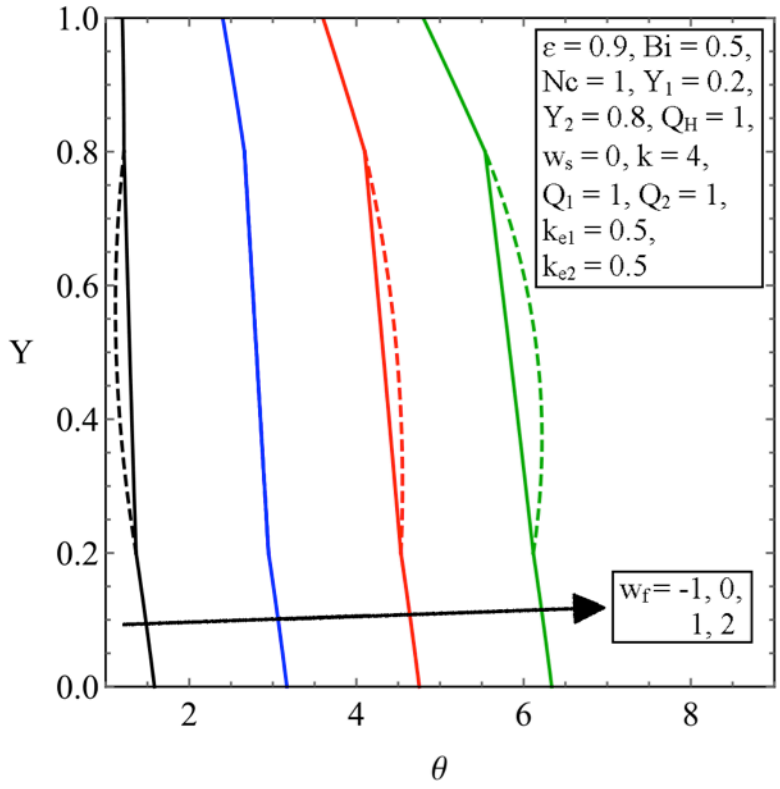

Fig. 5. Temperature distribution with various values for internal heat generation through the fluid medium: (a) Case one, (b) Case two.

1

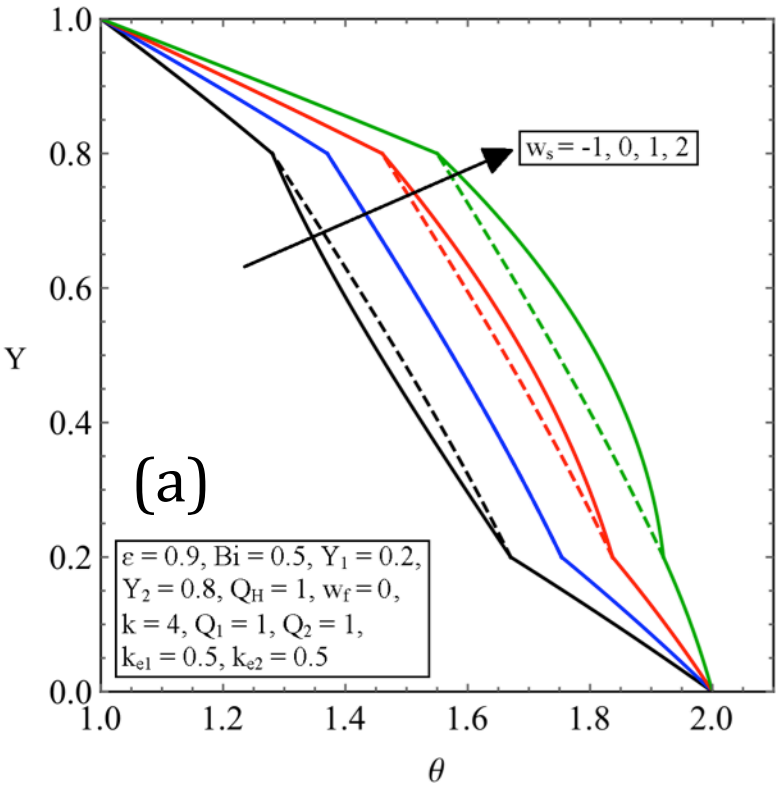
1.0
0.8
0.6
0.4
0.2
0.0
Y
1.0
1.2
1.4
1.6
1.8
2.0
θ
(a)
w_s = -1, 0, 1, 2
ε = 0.9, Bi = 0.5, Y_1 = 0.2,
Y_2 = 0.8, Q_H = 1, w_f = 0,
k = 4, Q_1 = 1, Q_2 = 1,
k_{e1} = 0.5, k_{e2} = 0.5

2

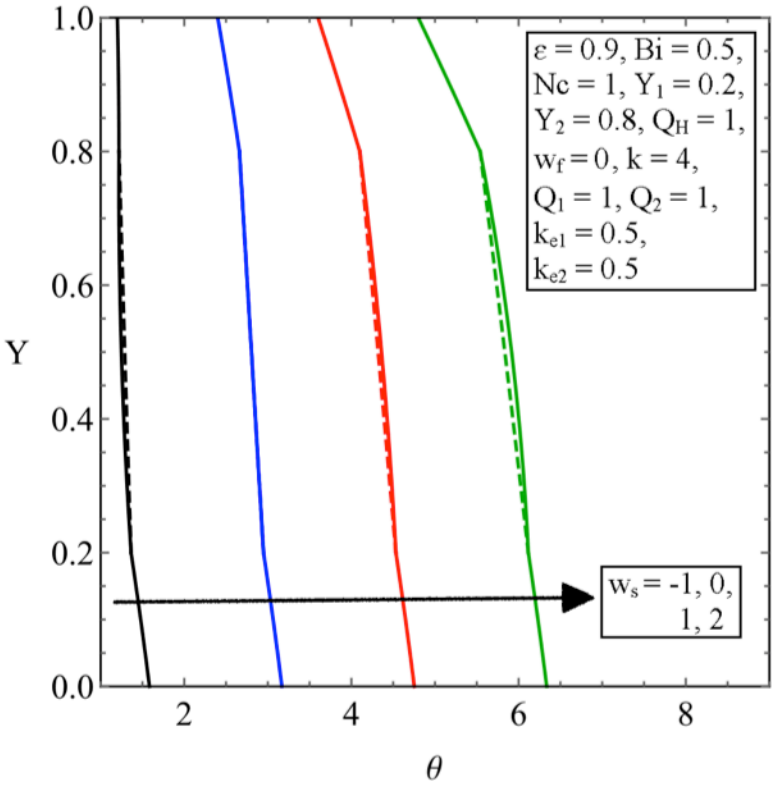
1.0
0.8
0.6
0.4
0.2
0.0
Y
2
4
6
8
θ
ε = 0.9, Bi = 0.5,
Nc = 1, Y_1 = 0.2,
Y_2 = 0.8, Q_H = 1,
w_f = 0, k = 4,
Q_1 = 1, Q_2 = 1,
k_{e1} = 0.5,
k_{e2} = 0.5
w_s = -1, 0,
1, 2

3

4

Fig. 6. Temperature distribution with various values for internal heat generation through the solid medium: (a) Case one, (b) Case two.

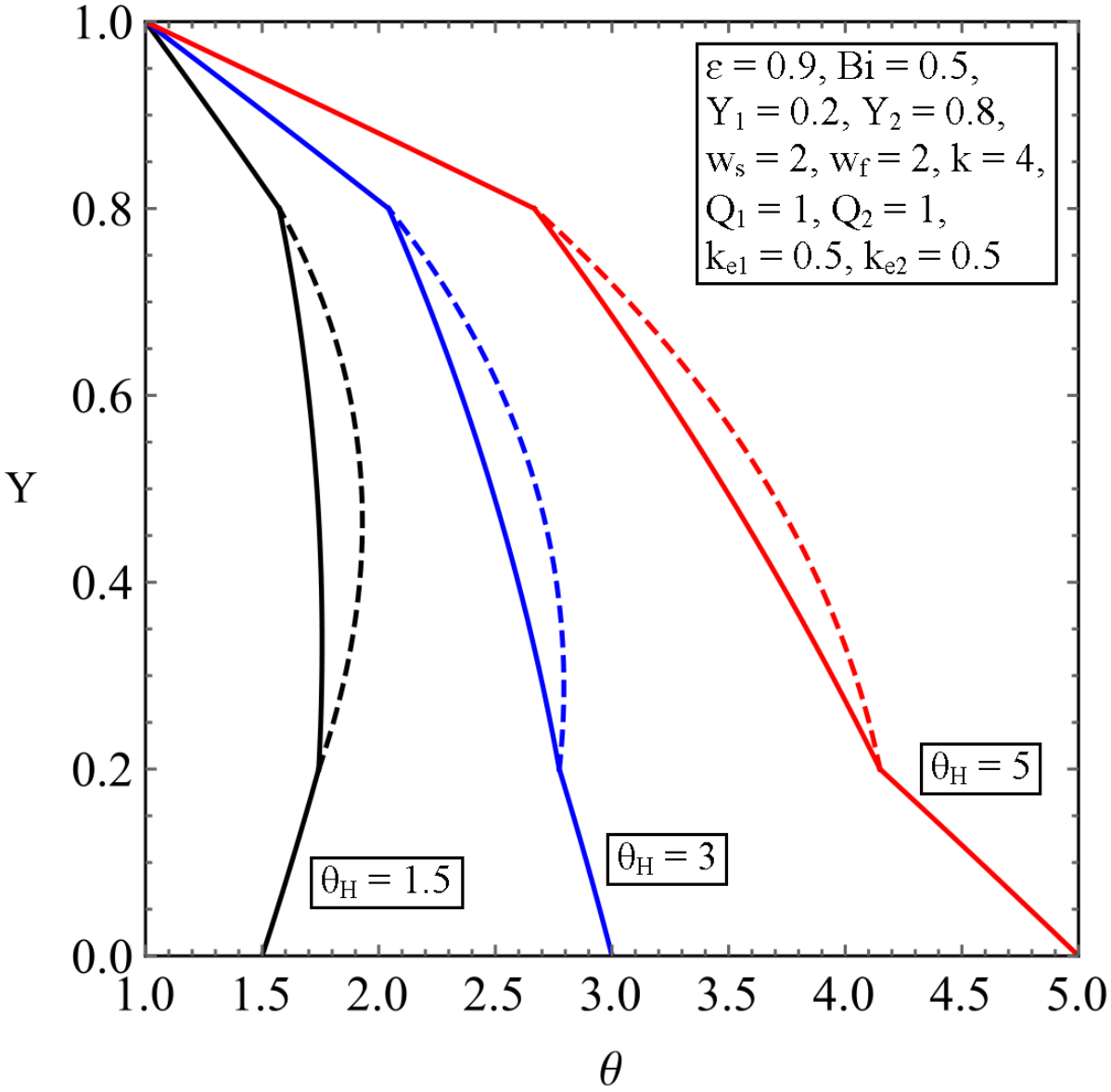

Fig. 7. Temperature distribution with various values for the hot temperature boundary condition (Case one).

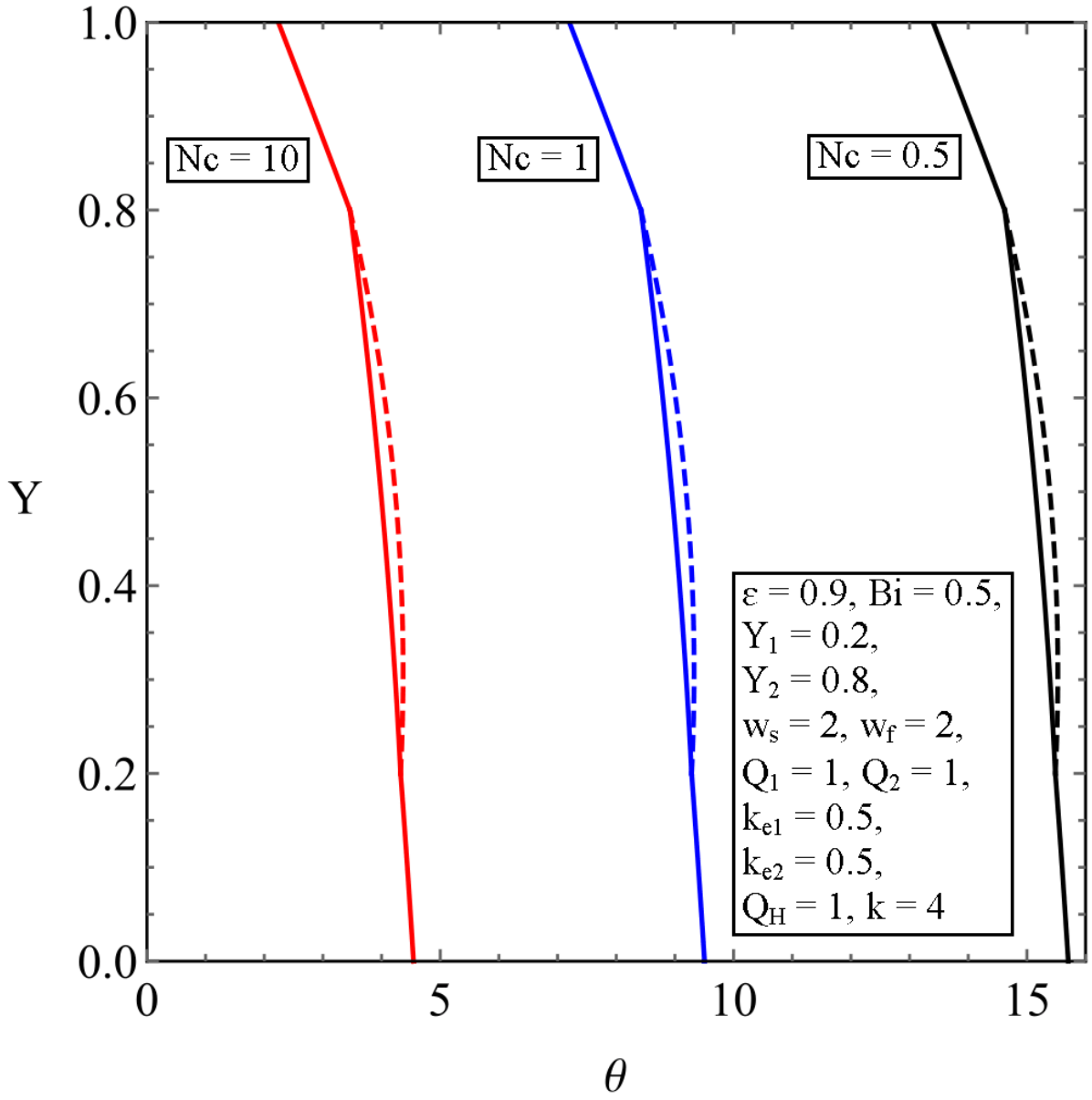

Fig. 8. Temperature distribution with various values for the convection boundary condition (Case two).

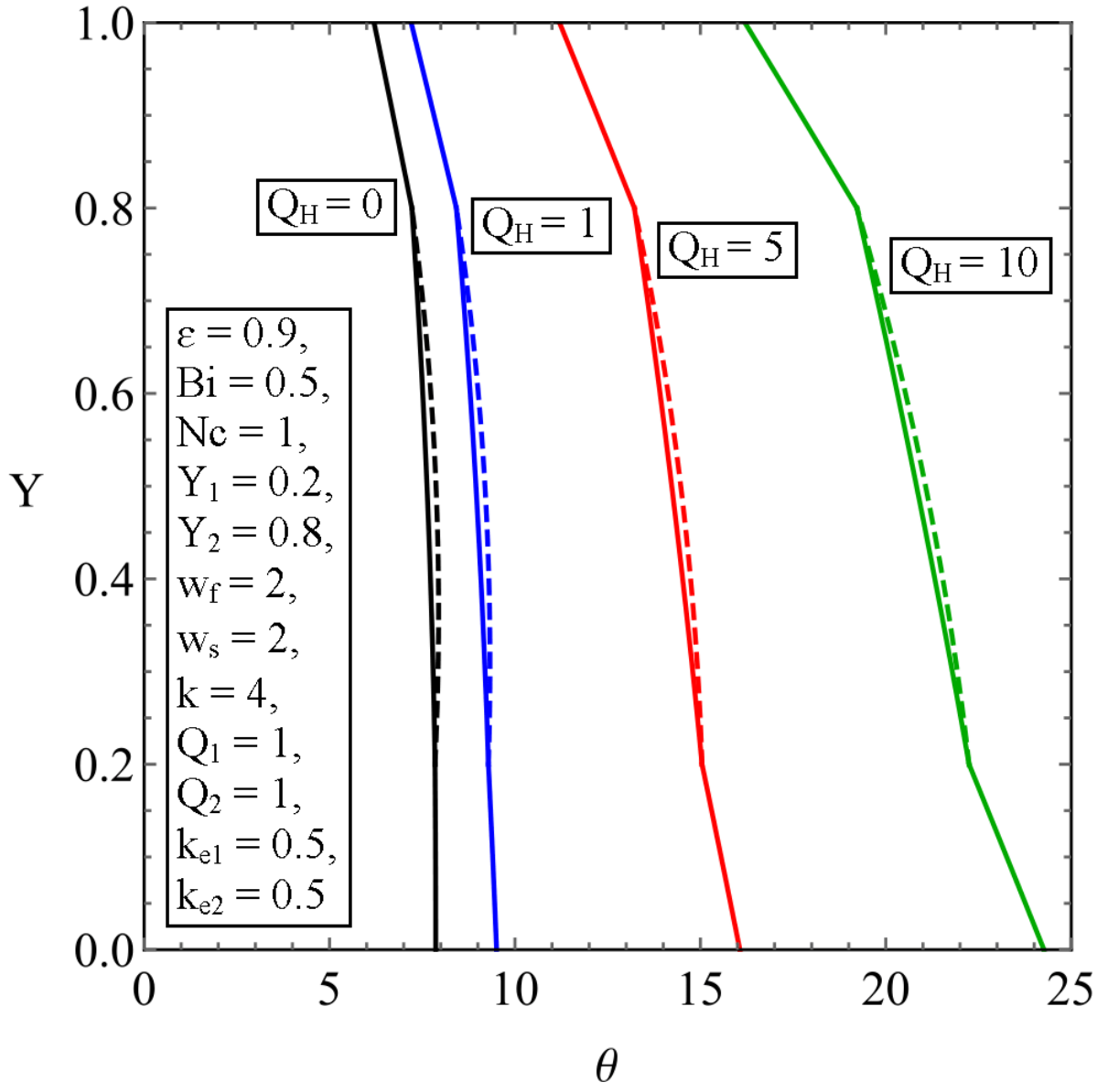

Fig. 9. Temperature distribution with various values for the heat flux boundary condition (Case two).

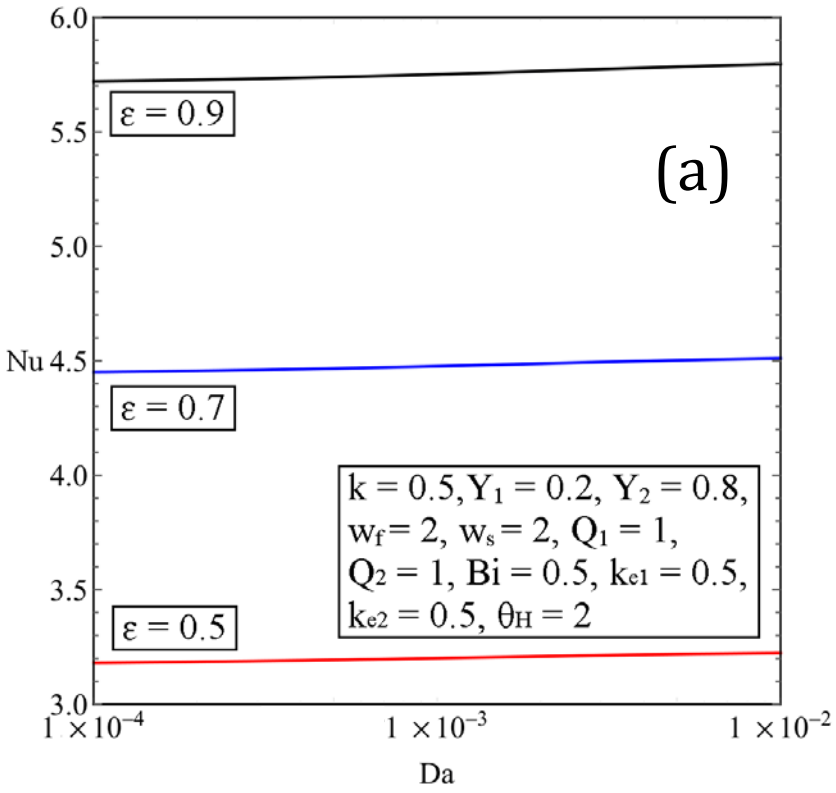

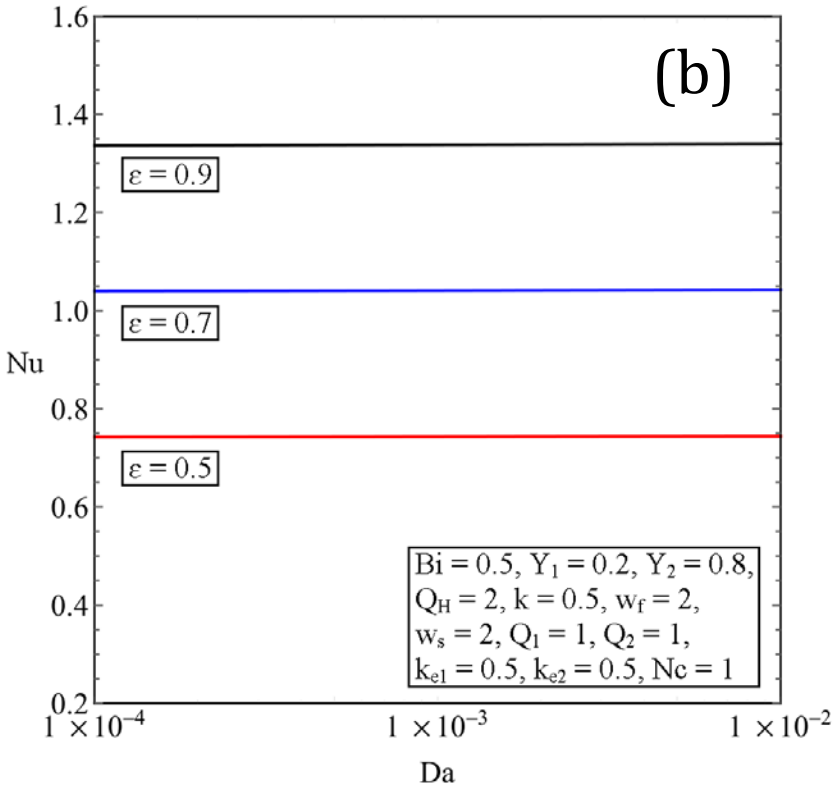

Fig. 10. Variation in Nusselt number versus Darcy number with various values of porosity: (a) Case one, (b) Case two.

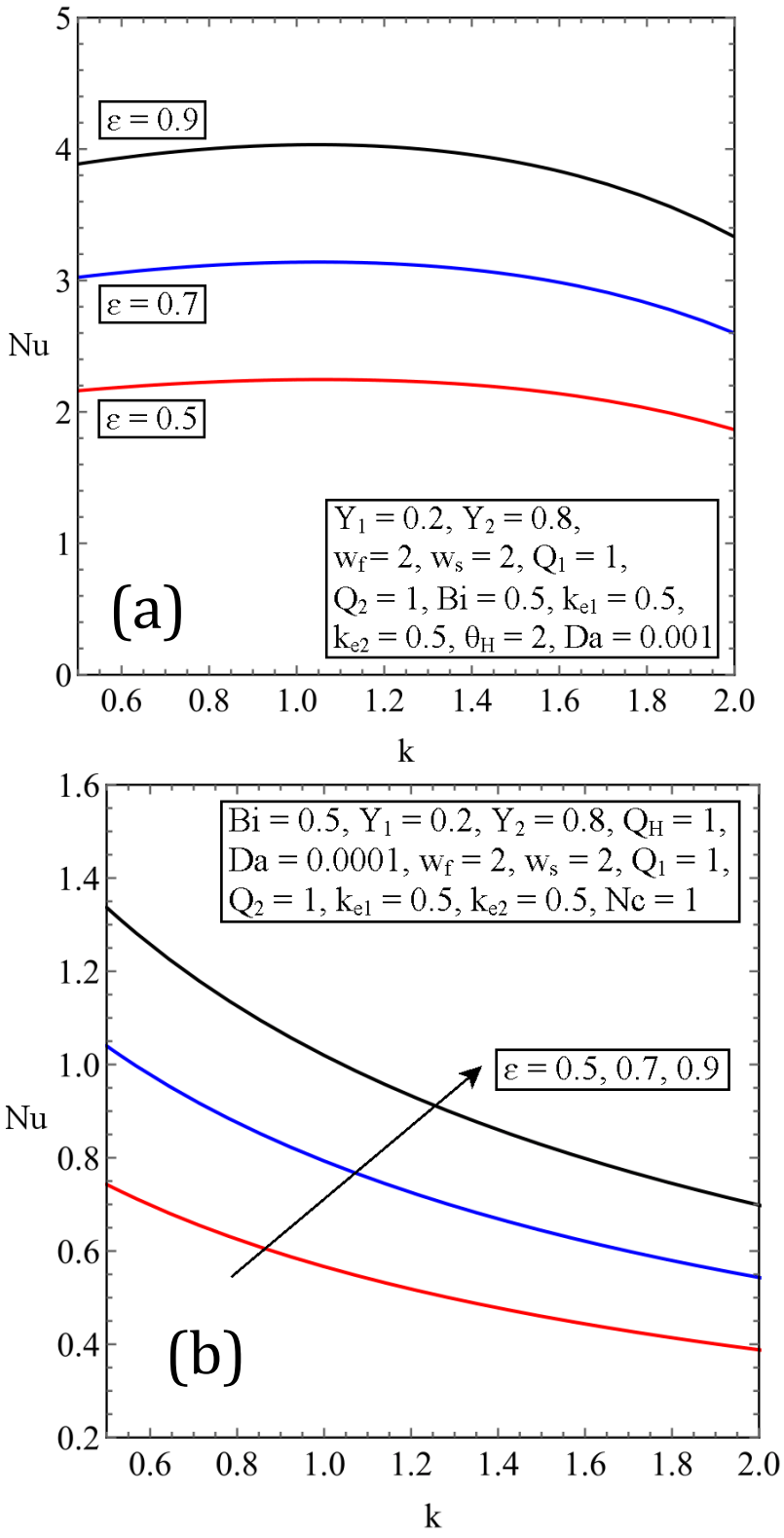

Fig. 11. Variation in Nusselt number versus thermal conductivity ratio with various values of porosity: (a) Case one, (b) Case two.

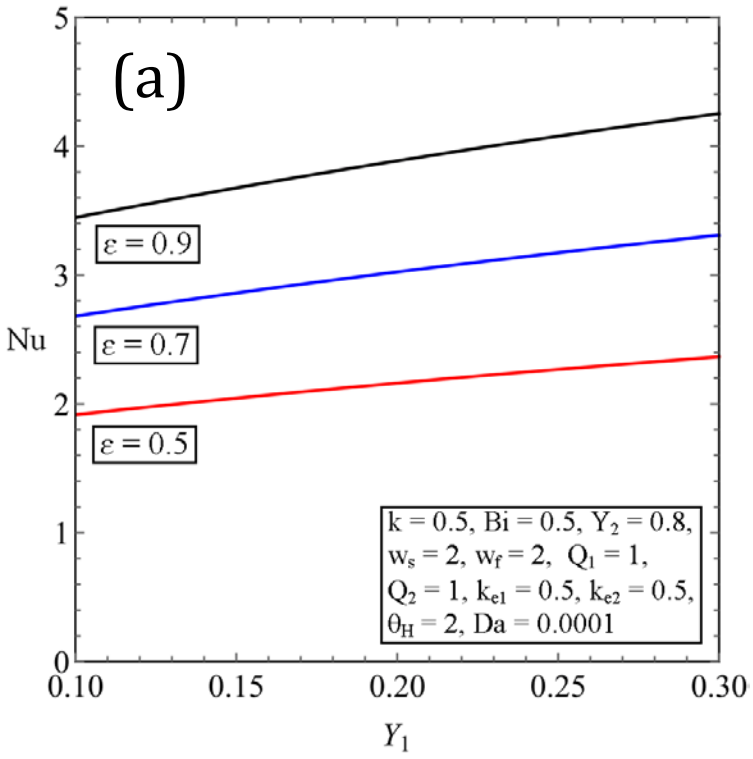

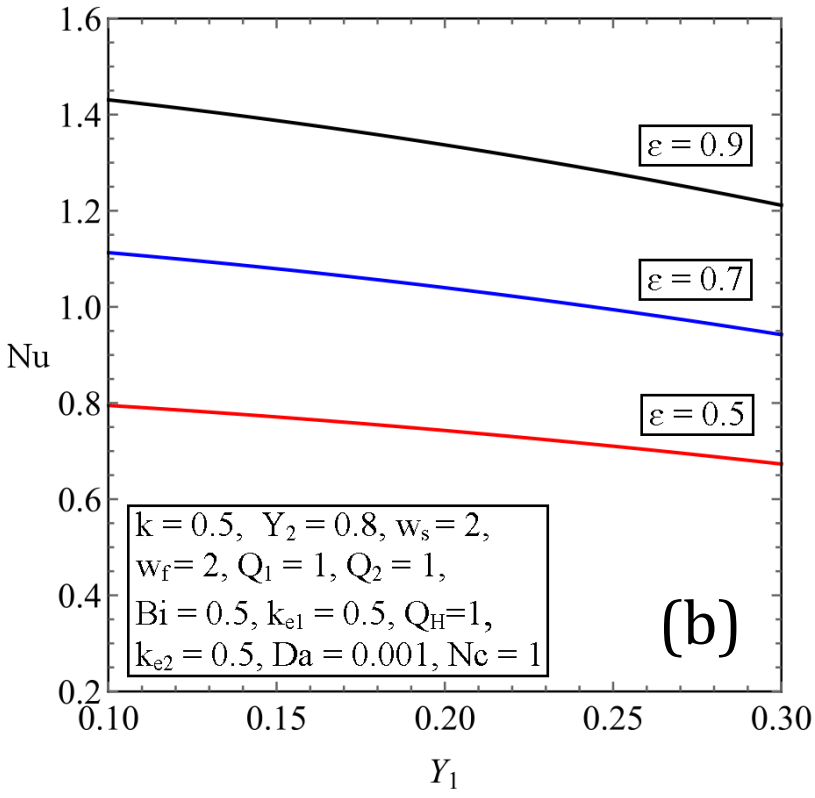

Fig. 12. Variation in Nusselt number versus lower wall thickness with various values of porosity: (a) Case one, (b) Case two.

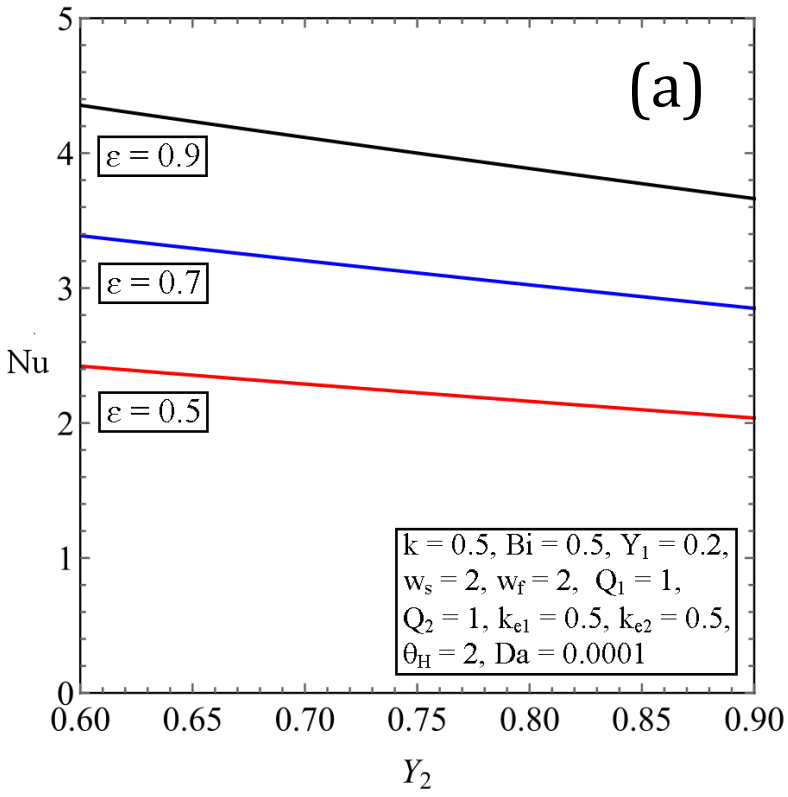

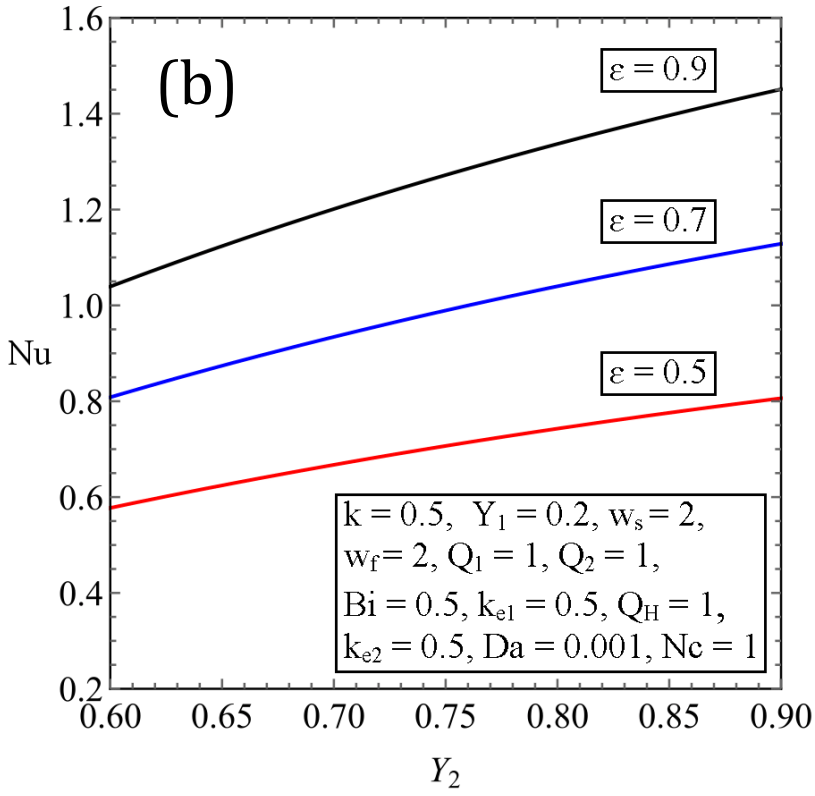

Fig. 13. Variation in Nusselt number versus upper wall thickness with various values of porosity: (a) Case one, (b) Case two.

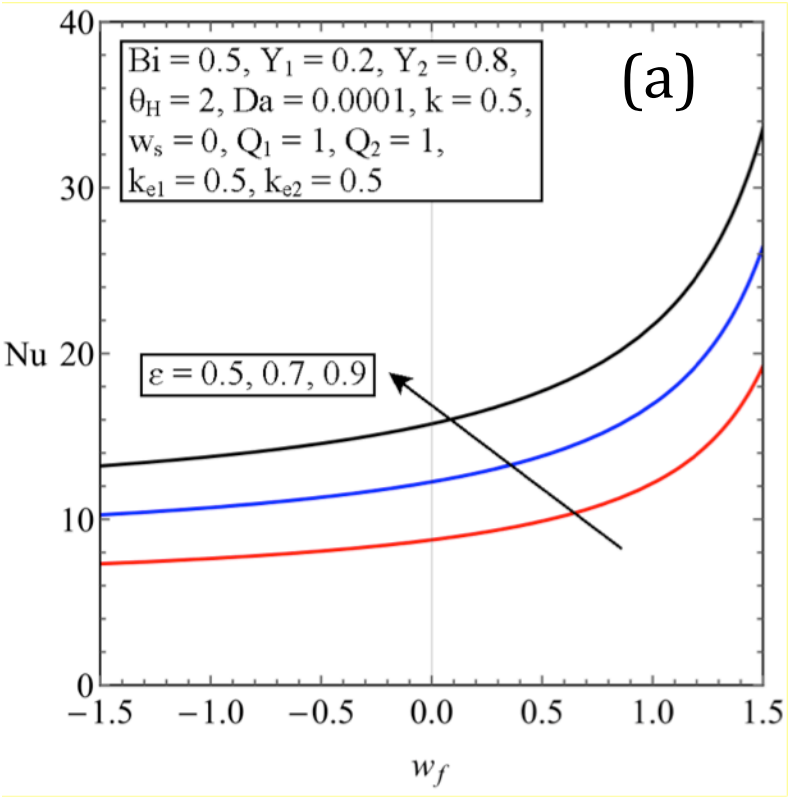

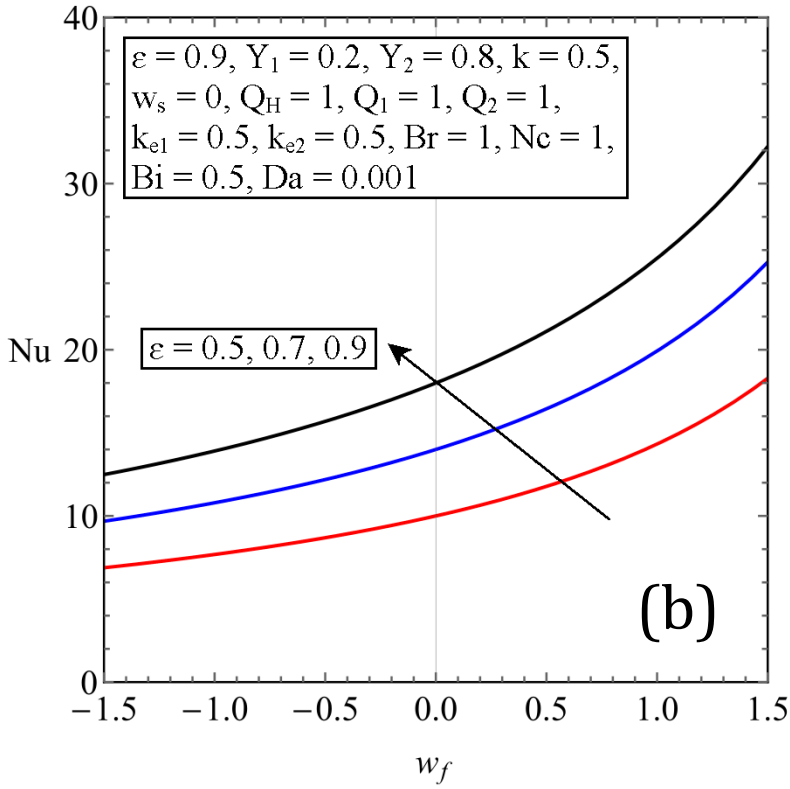

Fig. 14. Variation in Nusselt number versus internal heat generation through the fluid phase with various values of porosity: (a) Case one, (b) Case two.

1

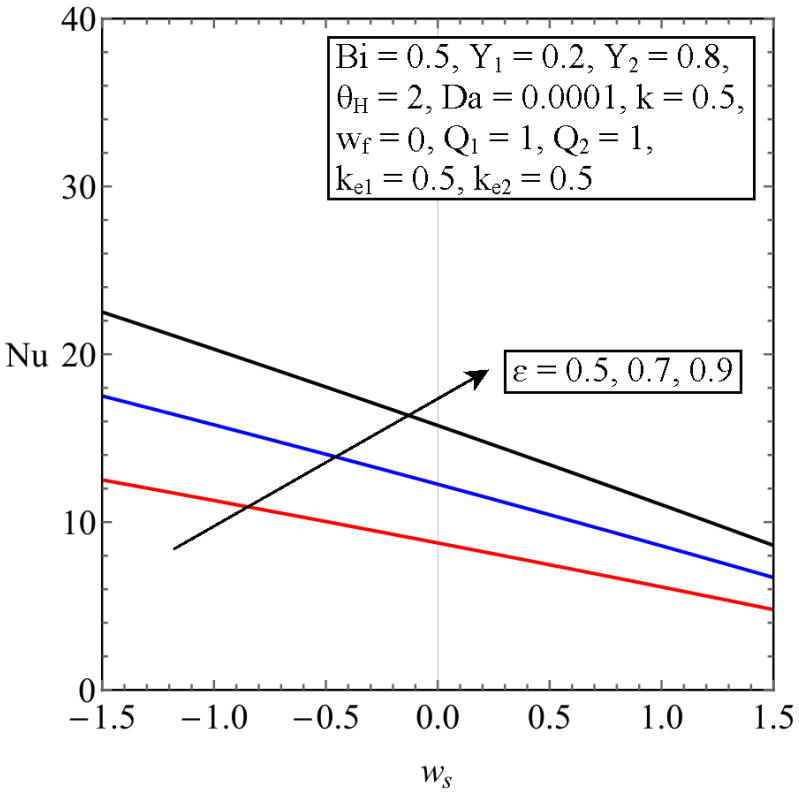
Bi = 0.5, Y1 = 0.2, Y2 = 0.8,
θH = 2, Da = 0.0001, k = 0.5,
wf = 0, Q1 = 1, Q2 = 1,
ke1 = 0.5, ke2 = 0.5
ε = 0.5, 0.7, 0.9
Nu
40
30
20
10
0
−1.5
−1.0
−0.5
0.0
0.5
1.0
1.5
ws

2

3

(a)

(b)

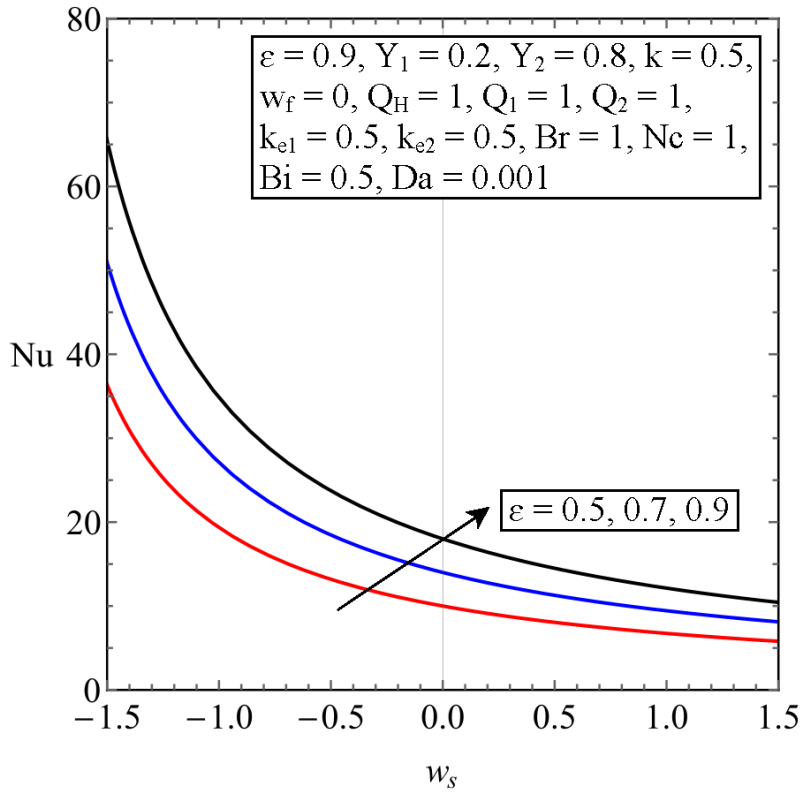

Fig. 15. Variation in Nusselt number versus internal heat generation through the solid phase with various values of porosity: (a) Case one, (b) Case two.